Catalysis Communications 47 (2014) 1–6

Contents lists available at ScienceDirect

Catalysis Communications

journal homepage: www.elsevier.com/locate/catcom

Short Communication

Photocatalytic hydrogen production by Au–M_xO_y (M=Ag, Cu, Ni) catalysts supported on TiO_2

Socorro Oros-Ruiz [a,b,*], Rodolfo Zanella [a,**], Sebastián E. Collins [c], Agileo Hernández-Gordillo [d], Ricardo Gómez [b]

[a] Centro de Ciencias Aplicadas y Desarrollo Tecnológico, Universidad Nacional Autónoma de México, Circuito Exterior S/N, Ciudad Universitaria, A. P. 70-186, Delegación Coyoacán, C.P. 04510, México DF, Mexico
[b] Universidad Autónoma Metropolitana-Iztapalapa, Departamento de Química, ECOCATAL, Av. San Rafael Atlixco No. 186, C.P. 09340, México, DF, Mexico
[c] Instituto de Desarrollo Tecnológico para la Industria Química (INTEC), Universidad Nacional del Litoral — CONICET, Güemes 3450, 3000 Santa Fe, Argentina
[d] CIIEMAD, Instituto Politécnico Nacional, Barrio la Laguna Ticomán, C.P. 07340 México, DF Mexico

ARTICLE INFO

Article history:
Received 31 October 2013
Received in revised form 24 December 2013
Accepted 28 December 2013
Available online 3 January 2014

Keywords:
TiO_2–metal oxide modification
Gold nanoparticles
Photocatalysis
Water splitting
Hydrogen production

ABSTRACT

Au–M_xO_y (M=Ag, Cu, Ni) nanoparticles supported on TiO_2–P25 were prepared by the deposition–precipitation method and were evaluated for the photocatalytic water splitting reaction for hydrogen production, using a mixture of water–methanol (1:1). The combinations of Au–Cu_2O/TiO_2 and Au–NiO/TiO_2 effectively increased the hydrogen production (2064 and 1636 $\mu mol \cdot h^{-1} \cdot g^{-1}$) obtained by Au/TiO_2 (1204 $\mu mol \cdot h^{-1} \cdot g^{-1}$). The higher photoactivities achieved by Au–Cu_2O and Au–NiO nanoparticles deposited on TiO_2 were attributed to an enhancement of the electron charge transfer from TiO_2 to the Au–M_xO_y systems and the effect of surface plasmon resonance of gold nanoparticles.

1. Introduction

The need to develop new alternatives for sustainable energy has drawn the attention to emergent clean renewable technologies, since they proceed from natural and lasting sources like solar light, wind and geothermal energy [1]. The alternative method of photocatalytic water splitting is promising since it involves the absorption of light to produce hydrogen by irradiating oxide semiconductors. Photocatalytic systems for water splitting may contain sacrificial reagents, as methanol, commonly used in the photocatalytic evolution of H_2 from water, since its hydroxy group captures photogenerated holes and minimizes the probability of e^-/h^+ recombination [2]. The incorporation of metals or metal oxide nanoparticles on the surface of semiconductors as cocatalysts has proved to enhance the photoactivity for the water splitting reaction [3,4]. These photocatalysts must be efficient, stable, harmless, abundant and inexpensive. In that way, metal oxides have been recently reported as efficient catalysts for photoreforming of alcohol solutions [5,6]. On the other hand, Au/TiO_2 has been reported as an effective monometallic photocatalyst for hydrogen production from an aqueous solution in the presence of methanol as hole scavenger [7–10]. In addition, it is known that the physical and chemical properties of supported bimetallic catalysts, or $Au/M_xO_y/TiO_2$ systems, are usually different from their single metal counterparts and they significantly vary as a function of the composition and particle size. Catalytic activity and selectivity of bimetallic systems can be found to be superior to either of the corresponding monometallic catalysts [11–13]. Moreover the presence of a second metal or metal oxide can induce geometric modifications of the surface of the gold particles [14,15]. In this work, the photocatalytic production of hydrogen by water splitting using Au–M_xO_y nanoparticles deposited on TiO_2–P25 is reported and compared to the hydrogen production of the corresponding Au and M_xO_y nanoparticles on TiO_2 to evaluate the effect of combining Au with Ag_2O, Cu_2O, or NiO as cocatalysts on TiO_2. The photocatalysts were characterized by UV–vis diffuse reflectance, TEM, ICP, EDS and XPS. The photocatalytic reactions were carried out by using a water–metanol mixture, 50–50% vol., and a low-energy mercury lamp (2.2 mW/cm^2).

2. Experimental

2.1. Preparation of Au/TiO_2 and M_xO_y/TiO_2 photocatalysts

Titania Degussa P25 was used as support (55 $m^2 \cdot g^{-1}$, nonporous, 70% anatase and 30% rutile, purity >99.5%). $HAuCl_4 \cdot 3H_2O$, $AgNO_3$,

* Correspondence to: S. Oros-Ruiz, Centro de Ciencias Aplicadas y Desarrollo Tecnológico, Universidad Nacional Autónoma de México, Circuito Exterior S/N, Ciudad Universitaria, A. P. 70-186, Delegación Coyoacán, C.P. 04510, México DF, Mexico. Tel.: +52 5556228635.
** Corresponding author. Tel.: +52 5556228635.
E-mail addresses: socorro.oros@ccadet.unam.mx (S. Oros-Ruiz), rodolfo.zanella@ccadet.unam.mx (R. Zanella).

1566-7367/$ – see front matter © 2013 Elsevier B.V. All rights reserved.
http://dx.doi.org/10.1016/j.catcom.2013.12.033

$Cu(NO_3)_2 \cdot 2.5H_2O$ and $Ni(NO_3)_2 \cdot 6H_2O$, all from Aldrich, were used as metal precursors. The preparation of Au/TiO_2–P25, Cu_2O/TiO_2–P25, and NiO/TiO_2–P25 was performed by deposition–precipitation using urea (DPU), following the previously reported procedure [16]. Briefly, the metal precursor (4.2×10^{-3} M) and urea (0.42 M for Au and 0.21 M for Cu and Ni) were dissolved in distilled water; then, 3 g of titania was added to this solution at 80 °C and kept constant for 16 h under stirring.

The Ag_2O/TiO_2–P25 photocatalyst was prepared by deposition–precipitation using NaOH, for that 3 g of TiO_2 was added to an aqueous solution containing $AgNO_3$ ($4.2 \cdot 10^{-3}$ M). The solution was heated at 80 °C, and the initial pH was ~3; then, it was adjusted to 9 by dropwise addition of NaOH (0.5 M). The suspension was vigorously stirred for 2 h at 80 °C.

After the deposition–precipitation procedure, all samples were centrifuged, washed with 300 mL of distilled water at 50 °C, centrifuged four times, and dried under vacuum for 2 h at 80 °C. After drying, the samples were stored at room temperature in a desiccator under vacuum, away from light in order to prevent any alteration.

2.2. Preparation of Au–M_xO_y/TiO_2 photocatalysts

For these samples, the gold nominal loading was fixed at 0.5 wt.%, the optimal gold loading previously obtained for the production of hydrogen using Au/TiO_2 photocatalysts [10], whereas for Ag, Cu or Ni was fixed to synthesize Au–M_xO_y/TiO_2 catalysts with theoretical atomic ratio Au:M of 1:1. A sequential deposition of the methods previously mentioned in Section 2.1 was used to prepare the Au–M_xO_y/TiO_2 materials [14,15]. The thermal treatment of the monometallic and bimetallic samples was made with a heating rate of 2 °C/min up to 300 °C for 2 h under air flow of 1 mL/mg of catalyst.

2.3. Characterization

To estimate the band-gap energy of the photocatalysts (E_g), a Cary 100 Scan spectrophotometer by Varian equipped with an integrating sphere (Labsphere DRA-CA-30I) was used. The chemical analysis of the catalysts was determined by ICP on a Perkin Elmer Optical Emission Spectrometer Optima 4300 DV and by electron dispersion spectroscopy (EDS) using a Scanning Electron Microscope JEOL 5900-LV with microanalysis on an EDS Oxford ISIS. The determination of the metallic particle size was performed by transmission electron microscopy (TEM) on a JEOL JEM 2010 operated at 200 keV. Particle size distributions and average particle size were determined by measuring about 300 particles from each sample. X-ray photoelectron spectroscopy (XPS) analyses were performed on a multi-technique (SPECS) equipment with a dual X-ray Mg/Al source and an hemispheric analyzer PHOIBOS 150. The spectra were obtained using pass energy of 30 eV, and the Al–KαX-ray source was operated at 100 W. The working pressure in the analyzing chamber was less than 2×10^{-8} mbar. The binding energies (BE) were referenced to the C (1s) peak fixed at 284.6 eV.

2.4. Evaluation of the photocatalytic activity for hydrogen production

The photocatalytic activity of the monometallic Au/TiO_2, Ag_2O/TiO_2, Cu_2O/TiO_2, and NiO/TiO_2 as well as the Au–Ag_2O/TiO_2, Au–Cu_2O/TiO_2, and Au–NiO/TiO_2 catalysts were studied in a homemade photoreactor containing 100 mg of catalyst in a volume of 200 mL of a water–methanol mixture (1:1 M ratio). The irradiation source was an UV–PC mercury lamp with primary emission at 254 nm with an intensity of 2.2 mW/cm^2; the determinations of hydrogen were made in a Shimadzu G-08 gas chromatograph with a thermal conductivity detector (TCD) using a ShinCarbon packed column (2 m length, 1 mm ID and 25 mm OD). The reaction was monitored for 10 h. To assure the homogenization of the system, the mixture reaction was stirred in the dark for 30 min and degassed by bubbling nitrogen prior to the photochemical reaction.

3. Results and discussion

3.1. Elemental analysis

Table 1 compares the nominal and the measured metal loadings in wt. % and the Au:M atomic ratios for the Au–M_xO_y samples. As expected from former studies on gold catalysts [16,17], the actual gold loadings are very close to the theoretical value (0.5 wt.%), whether the catalyst is mono or bimetallic. In the case of copper, silver, and nickel oxide nanoparticles, the metal loadings showed good agreement with the nominal values as reported in Table 1, confirming that metal oxide nanoparticles of Cu, Ag, and Ni were not leached during Au deposition.

3.2. Oxidation state of the metals in the photocatalysts

Fig. 1 presents the XPS spectra collected from the samples previously calcined at 300 °C under air flow. For all samples, the Ti 2p spectrum showed two components at binding energies (BE) $2p_{3/2}$ 457.8 eV and $2p_{1/2}$ 463.2 eV characteristic of Ti^{4+}. XPS peaks in the gold 4f region were fitted with Doniach–Sunjic type curves [18]. The position of the Au 4f peaks, both in monometallic and bimetallic photocatalysts, showed that for each case the characteristic signal $4f_{7/2}$ is in the range of 82.8 and 83.2 eV (Fig. 1A). The position of that signal is slightly lower than bulk gold, and it is usually assigned to small gold particles in metallic state on reducible oxides, such as TiO_2 [18–20]. It has been reported that gold precursor after DPU synthesis decomposes upon thermal treatment, either in oxidant or reductant atmosphere, due to the instability of gold oxide [18].

The XPS spectra of Ag/TiO_2 and Au–Ag/TiO_2 catalysts present peaks of Ag $3d_{3/2}$ and $3d_{5/2}$ at 373.0 and 367.1 eV, at 373.4 and 367.4 eV, respectively. The position of these signals are close to those attributed to silver oxides, AgO (367.05 eV) and Ag_2O (367.6 eV), but not to metallic silver (368.3 eV) [21]. See Fig. 1B. Moreover, in order to assess the oxidation state of silver in these catalysts, the Auger parameter was calculated as: α = BE (Ag $3d_{5/2}$) + KE (Ag M_4VV). The obtained values are

Table 1
Metal loading of the Au, M_xO_y or Au–M_xO_y on TiO_2 photocatalysts evaluated for hydrogen production.

Photocatalyst	E_g (eV)	Au loading (wt. %)	M loading (wt. %)	Au, M_xO_y or Au–M_xO_y particle size (nm)	Hydrogen production ($\mu mol \cdot h^{-1} \cdot g$ of catalyst^{-1})
TiO_2–P25	3.1	–	–	–	17
Au/TiO_2–P25	3.0	0.48	–	2.0 ± 0.3	1204
Ag_2O/TiO_2–P25	3.0	–	0.49	1.8 ± 0.3	202
Cu_2O/TiO_2–P25	3.1	–	0.47	2.1 ± 0.2	842
NiO/TiO_2–P25	3.0	–	0.45	1.8 ± 0.2	680
Au–Ag_2O/TiO_2–P25	2.9	0.47	0.22	2.6 ± 0.1	980
Au–Cu_2O/TiO_2–P25	3.0	0.46	0.15	2.5 ± 0.1	2064
Au–NiO/TiO_2–P25	2.9	0.46	0.16	2.5 ± 0.2	1636

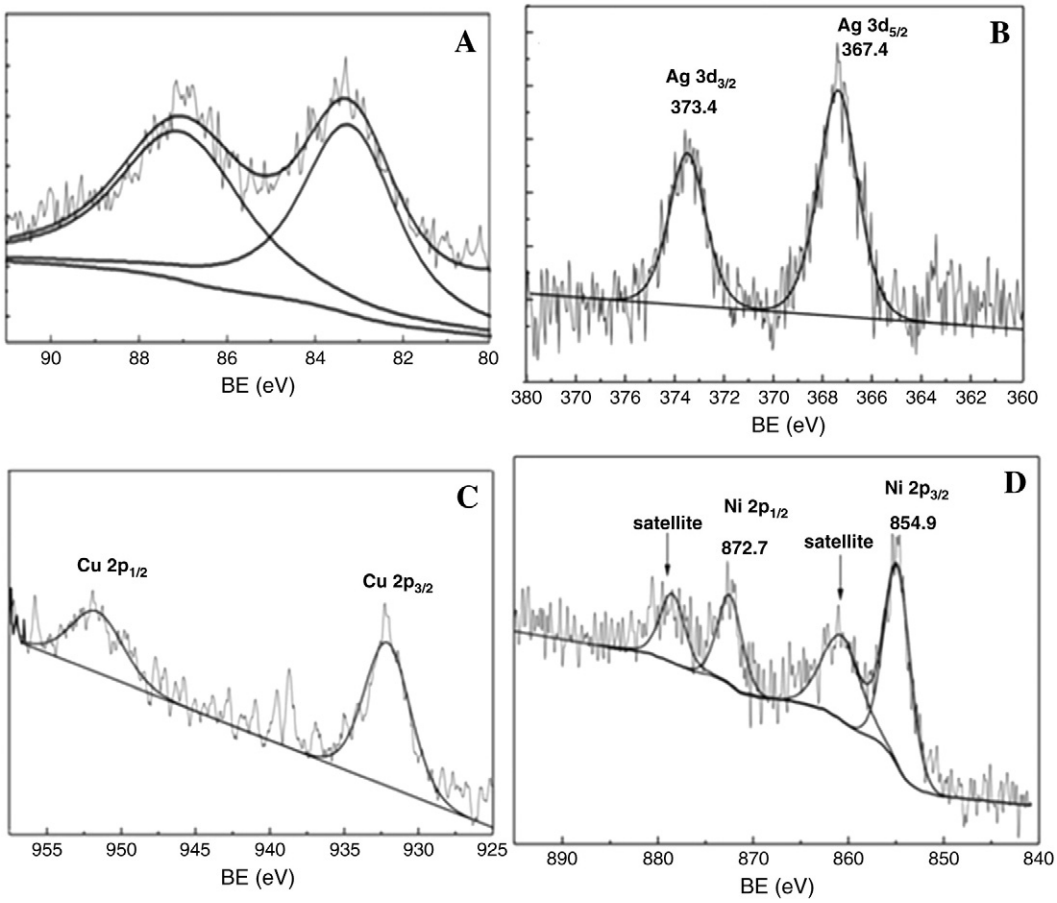

Fig. 1. XPS spectra of the different catalysts evaluated for hydrogen production: A) Au/TiO2, B) Au–Ag2O/TiO2, C) Au–Cu2O/TiO2 and D) Au–NiO/TiO2.

closer to those reported for Ag^{1+} [6,22,23] with $\alpha = 724.3$ eV, being then Ag_2O the main silver species.

The XPS spectrum of the bimetallic Au–Cu_2O/TiO_2 catalyst is presented in Fig. 1C; it shows typical doublet at 951.6 and 932.1 eV in the Cu 2p region. The position and splitting ($\Delta BE = 20$ eV) of these peaks point to the presence of Cu^{1+}, as Cu_2O, but because of the low signal-to-noise ratio, we cannot rule out a minor amount of metallic copper [24]. The presence of Cu^{2+} can be excluded because of the absence of the characteristic shake-up satellite lines of CuO [25].

The monometallic sample of NiO/TiO_2 presented signals in the 2d region corresponding to Ni $2p_{3/2}$ and Ni $2p_{1/2}$, at 854.9 and 872.7 eV, respectively, along with the corresponding satellite peaks at 860.9 and 878.7 eV [21]. See Fig. 1D. These signals can be ascribed to the presence of NiO and/or $Ni(OH)_2$, and presented a good agreement with literature [21,26].

3.3. Optical properties of photocatalysts

The UV–vis diffuse reflectance spectra for the photocatalysts containing monometallic nanoparticles supported on titania are presented in Fig. 2A. The photocatalyst containing gold nanoparticles in metallic form (Au/TiO_2) presents a typical absorption band in the visible region from 500 to 600 nm with a maximum at 550 nm. This signal is generated by the plasmonic resonance of light on the surface of the metallic

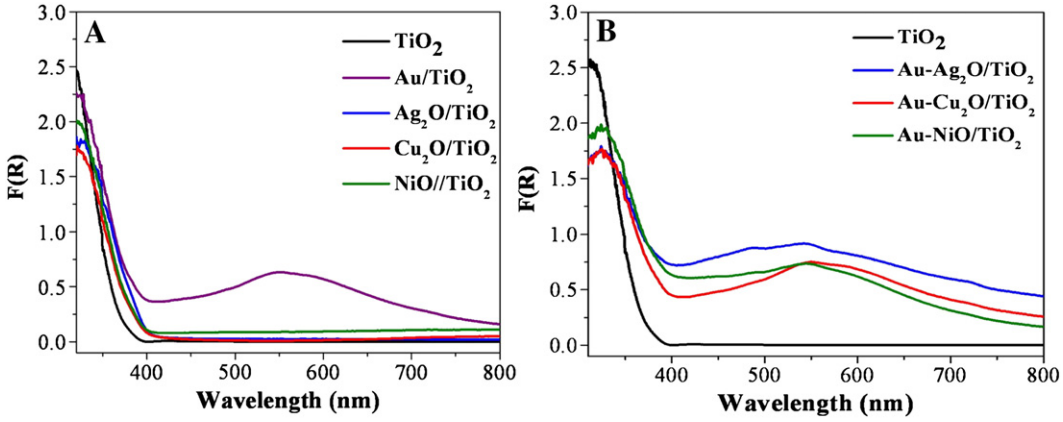

Fig. 2. UV–vis absorption spectra of the photocatalysts: A) Au and M_xO_y at 0.5 wt.% of metal loading B) Au–M_xO_y particles with atomic ratio Au:M 1:1.

nanoparticles of gold [28]. The samples containing metal oxides of Ag, Cu, and Ni did not exhibit this intense absorption for the same metal loading since they appeared in oxidized state after the thermal treatment process, as confirmed by the XPS analysis.

Fig. 2B shows the UV–vis diffuse reflectance spectra for the TiO_2 photocatalysts containing Au–M_xO_y nanoparticles. In all cases, an absorption band in the visible region is observed, with maximum absorptions located at 542, 550 and 547 nm for the Au–Ag_2O, Au–Cu_2O, and Au–NiO samples, respectively. These bands are attributed to metallic gold nanoparticles since, as observed from the metal oxide samples, Ag, Cu, and Ni in oxidized state do not present a plasmonic absorption [15]. The band-gap energies were calculated by the Kubelka-Munk (KM) method using the theory of optical absorption for indirect allowed transitions [27] and are summarized in Table 1. It is observed that the band-gap energy for the TiO_2 samples containing metal or metal oxide nanoparticles presents a slight displacement to lower energy values.

3.4. Particle size distribution

The particle size distribution and standard deviation were determined by measuring about 300 particles from each catalyst. Fig. 3 shows the particle size distribution for the Au and M_xO_y nanoparticles; Fig. 4 shows the particle size distribution for the Au–M_xO_y catalysts; the average particle size and standard deviations are reported in Table 1. The average particle size for Au and M_xO_y samples is close to 2 nm, whereas it is about 2.5 nm in the case of Au–M_xO_y/TiO_2 samples. These results indicate that the sequential deposition precipitation method allows a good control of the formation of nanoparticles. Moreover, the textural properties of the photocatalysts, determined by the BET method, were not altered by the metal incorporation; in all the cases, the BET surface area was about 55 m^2/g.

3.5. Hydrogen production of Au/TiO_2 and M_xO_y/TiO_2 nanoparticles supported on TiO_2

For comparative purposes, the metal loading was 0.5 wt.% for the Au/TiO_2 and M_xO_y/TiO_2 materials, this load was previously optimized for the photocatalytic hydrogen production in Au/TiO_2 catalysts [10]. The catalysts were evaluated under the same reaction conditions; the most active photocatalyst was Au/TiO_2 which produced about 1200 μmol/h·g after 10 h of reaction; and in decreasing order it was followed by Cu_2O/TiO_2 (838 μmol/h·g), NiO/TiO_2 (636 μmol/h·g), and, finally, the lowest activity for water splitting was obtained by the Ag_2O/TiO_2 photocatalyst (200 μmol/h·g). See Fig. 5A. The outstanding activity of Au^0 nanoparticles reported here is in agreement with previous reports [3,7] showing that gold nanoparticles are very efficient metallic co-catalysts for the water splitting reaction [8,9]. As determined by XPS, gold is present in the metallic form, whereas silver, copper, and nickel are deposited on TiO_2 in different oxidized states.

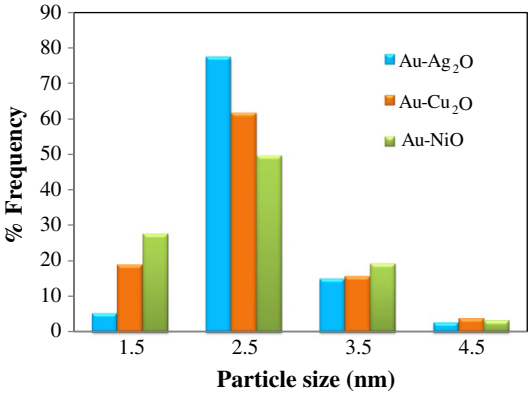

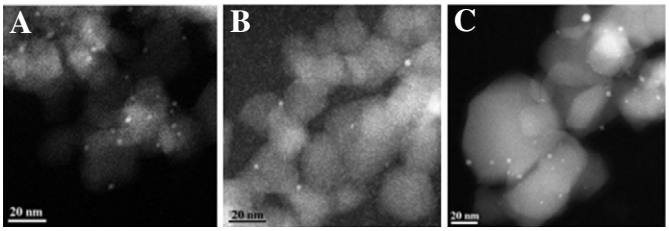

Fig. 4. Particle size distributions for the nanoparticles in the bimetallic photocatalysts and HAADF images of a) Au–Ag_2O/TiO_2, b) Au–Cu_2O/TiO_2, and c) Au–NiO/TiO_2.

The different activities obtained by these materials could be related to the work functions of the nanoparticles used as co-catalysts, as proposed by other authors, who found a correlation between the work function of the nanoparticles and their resulting photoactivity [29,30]. The electron transfer is facilitated from a material with a lower work function to another with a higher value of work function, where this last material acts as an efficient trap for the photogenerated electrons preventing the e^-/h^+ recombination and as consequence, improving the photocatalytic activity [31,32]. The work function values of TiO_2(−4.0 eV) allow an efficient electron transfer from TiO_2 to Au nanoparticles (−5.1 eV) [33]. Cu_2O(4.84 eV) [34] and NiO (5.2 eV) [35] present lower activity than Au nanoparticles, also enhancing the photoactivity of bare TiO_2. The lowest activity of the metal oxides evaluated as co-catalysts for water splitting was obtained by Ag_2O possessing the lowest value of work function (−4.7 eV) [33] (Fig. 5A).

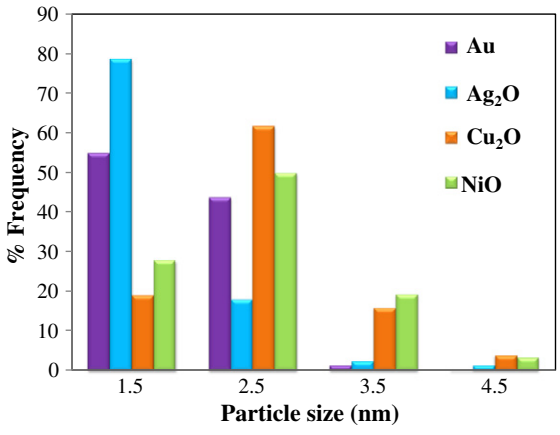

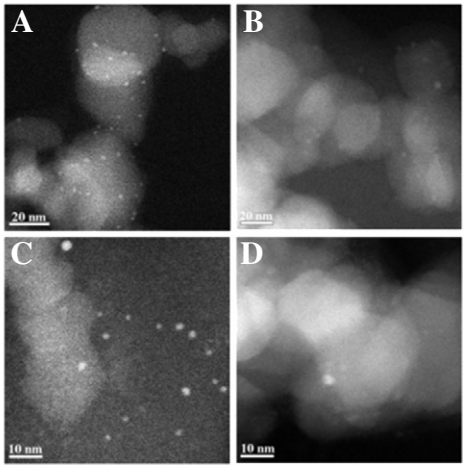

Fig. 3. Particle size distributions and HAADF images for photocatalysts: a) Au/TiO_2, b)Ag_2O/TiO_2, c) Cu_2O/TiO_2, and d) NiO/TiO_2.

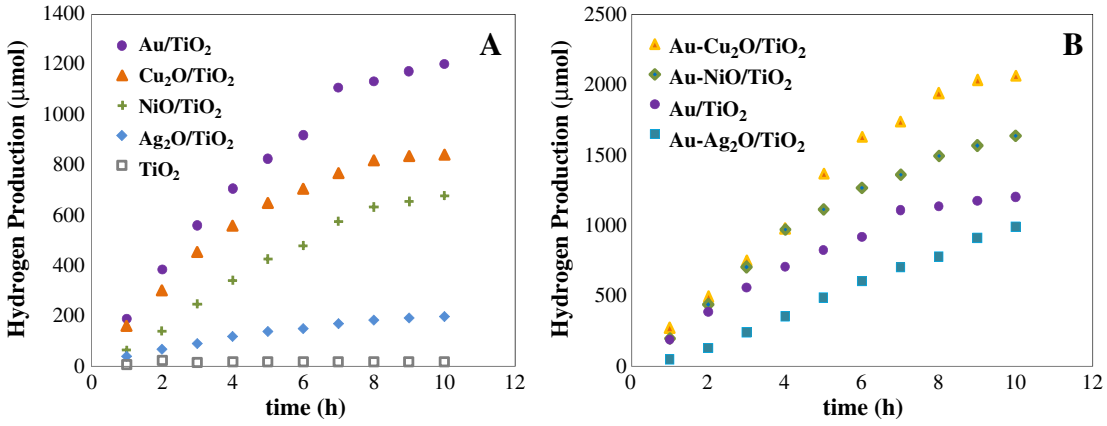

Fig. 5. Hydrogen production from A) Au and M_xO_y on TiO_2 at 0.5 wt.% photocatalysts and B) Au and Au–M_xO_y at Au:M 1:1, Au loading 0.5 wt.% photocatalysts.

On the other hand, it is known that surface plasmon resonance (SPR) of gold nanoparticles can generate enhanced localized electric fields, which may concentrate the light energy incident on the surface of composite and generate more photo-excited electrons nearby [36–38], that could also explain the highest photoactivity on the surface of Au/TiO_2. This enhancement has been previously observed and has been attributed to the strong electric fields created by the SPR of the Au nanoparticles, which excite electron–hole pairs locally in the TiO_2 at a rate several orders of magnitude higher than the normal incident light [37,38].

3.6. Hydrogen production using Au–M_xO_y/TiO_2 photocatalysts

The hydrogen production profiles of Au–M_xO_y/TiO_2 photocatalysts were evaluated and compared to the most active monometallic photocatalyst (Au/TiO_2); the results are shown in Fig. 5B. The combination of bimetallic catalysts of Au–Cu_2O and Au–NiO at 1:1 Au:M atomic ratio improved the production of hydrogen obtained by the most active catalyst Au/TiO_2 0.5 wt. %. The presence of gold and metal oxides like Cu_2O or NiO as co-catalysts on TiO_2 surface increased significantly the production of hydrogen by avoiding the recombination of the hole–electron pair and achieving the highest production of hydrogen. The Au–Ag_2O system had a detrimental effect compared to the Au/TiO_2 photocatalyst, inhibiting hydrogen production, probably because of a lower electron transfer charge from TiO_2 to the Au–Ag_2O system. Moreover Fig. 2B shows that SPR of Au is modified by the addition of metal oxides to the Au/TiO_2 system. It is well known that SPR is influenced, among other factors, by the surrounding environment of gold nanoparticles [36–38]. Modification of gold-SPR by the addition of metal oxides to the Au/TiO_2 catalyst may also explain the increased photoactivity of Au–Cu_2O/TiO_2 and Au–NiO/TiO_2 systems however a deeper study about this topic is necessary to reach solid conclusions.

4. Conclusions

The Au–Cu_2O and Au–NiO systems used as metal–metal oxide composite catalysts supported on TiO_2 increased effectively the production of hydrogen obtained by monometallic gold nanoparticles. The deposition of these metals on the surface of the semiconductor by sequential deposition produced well-dispersed and homogeneous metal oxide nanoparticles, showing a good activity for photocatalytic water splitting. The most active photocatalysts were Au–Cu_2O/TiO_2 and Au–NiO/TiO_2 with gold loadings of 0.5% and Au–M_xO_y atomic ratio Au:M of 1:1. The enhanced photoactivity was a result of the Au positive effect on the semiconductors surface for the electron transfer from TiO_2 to Au–metal oxide nanoparticles.

Acknowledgments

We acknowledge the financial support granted by CONACYT 130407, CONACYT–MINCYT 164346, and PAPIIT, UNAM, Mexico 103513. We would also like to thank ANPCyT for the SPECS multitechnique analysis instrument facilities (PME8-2003). Socorro Oros-Ruiz thanks to UNAM–DGAPA for the postdoctoral grant.

References

[1] N.L. Panwar, S.C. Kaushik, S. Kothari, Renew. Sust. Energy Rev. 15 (2011) 1513–1524.
[2] M. Cargnello, A. Gasparotto, V. Gombac, T. Montini, D. Barreca, P. Fornasiero, Eur. J. Inorg. Chem. 2011 (2011) 4309–4323.
[3] T. Sreethawong, S. Yoshikawa, Catal. Commun. 6 (2005) 661–668.
[4] M. Ni, M.K.H. Leung, D.Y.C. Leung, K. Sumathy, Renew. Sust. Energy Rev. 11 (2007) 401–425.
[5] C. Maccato, D. Barreca, G. Carraro, A. Gasparotto, V. Gombac, P. Fornasiero, Surf. Coat. Technol. 230 (2013) 219–227.
[6] Q. Simon, D. Barreca, D. Bekermann, A. Gasparotto, C. Maccato, E. Comini, V. Gombac, P. Fornasiero, O.I. Lebedev, S. Turner, A. Devi, R.A. Fischer, G. Van Tendeloo, Int. J. Hydrogen Energy 36 (2011) 15527–15537.
[7] M. Murdoch, G.I.N. Waterhouse, M.A. Nadeem, J.B. Metson, M.A. Keane, R.F. Howe, J. Llorca, H. Idriss, Nat. Chem. 3 (2011) 489–492.
[8] F. Gärtner, S. Losse, A. Boddien, M.-M. Pohl, S. Denurra, H. Junge, M. Beller, Chem. Sustain. Chem. 5 (2011) 530–533.
[9] C. Gomes Silva, R. Juárez, T. Marino, R. Molinari, H. García, J. Am. Chem. Soc. 133 (2011) 595–602.
[10] S. Oros-Ruiz, R. Zanella, R. López, A. Hernández-Gordillo, R. Gómez, J. Hazard Mater. 263 (2013) 2–10.
[11] J. Gong, Chem. Rev. 112 (2012) 2987–3054.
[12] C.L. Bracey, P.R. Ellis, G.J. Hutchings, Chem. Soc. Rev. 38 (2009) 2231–2243.
[13] R. Ferrando, J. Jellinek, R.L. Johnston, Chem. Rev. 108 (2008) 845–910.
[14] A. Sandoval, A. Aguilar, C. Louis, A. Traverse, R. Zanella, J. Catal. 281 (2011) 40–49.
[15] A. Sandoval, C. Louis, R. Zanella, Appl. Catal. B Environ. 140–141 (2013) 363–377.
[16] R. Zanella, L. Delannoy, C. Louis, Appl. Catal. A Gen. 291 (2005) 62–72.
[17] R. Zanella, S. Giorgio, C.R. Henry, C. Louis, J. Phys. Chem. B 106 (2002) 7634–7642.
[18] E. Del Río, G. Blanco, S. Collins, M.L. Haro, X. Chen, J.J. Delgado, J.J. Calvino, S. Bernal, Top. Catal. 54 (2011) 931–940.
[19] N. Kruse, S. Chenakin, Appl. Catal. A Gen. 391 (2011) 367–376.
[20] J. Radnik, C. Mohr, P. Claus, Phys. Chem. Chem. Phys. 5 (2003) 172–177.
[21] P. Prieto, V. Nistor, K. Nouneh, M. Oyama, M. Abd-Lefdil, R. Díaz, Appl. Surf. Sci. 258 (2012) 8807–8813.
[22] G.I.N. Waterhouse, G.A. Bowmaker, J.B. Metson, Appl. Surf. Sci. 183 (2001) 191–204.
[23] L. Armelao, D. Barreca, G. Bottaro, A. Gasparotto, C. Maccato, E. Tondello, O.I. Lebedev, S. Turner, G. Van Tendeloo, C. Sada, U.L. Štangar, Chem. Phys. Chem. 10 (2009) 3249–3259.
[24] R. López, R. Gómez, M.E. Llanos, Catal. Today 148 (2009) 103–108.
[25] C.D. Wagner, G.E. Muilenberg, in: Eden Praire (Ed.), Handbook of X-ray Photoelectron Spectroscopy: A Reference Book of Standard Data for Use in X-ray Photoelectron Spectroscopy, Physical Electronics Division Perkin-Elmer Corp, Minnesota, 1979.
[26] G.-P. Jin, Y.-F. Ding, P.-P. Zheng, J. Power Sources 166 (2007) 80–86.
[27] R. López, R. Gómez, J. Sol–gel, Sci. Technol. 61 (2012) 1–7.
[28] J.A. Reyes-Esqueda, A. Bautista-Salvador, R. Zanella, 8 (2008) 3843–3850.
[29] A. Naldoni, M. D'Arienzo, M. Altomare, M. Marelli, R. Scotti, F. Morazzoni, E. Selli, V. Dal Santo, Appl. Catal. B Environ. 130–131 (2013) 239–248.
[30] P. Gomathisankar, D. Yamamoto, H. Katsumata, T. Suzuki, S. Kaneco, Int. J. Hydrogen Energy 38 (2013) 5517–5524.

[31] N. Bowering, D. Croston, P.G. Harrison, G.S. Walker, Int. J. Photoenergy 8 (2007) Article ID 90752.
[32] T.T.Y. Tan, C.K. Yip, D. Beydoun, R. Amal, Chem. Eng. J. 95 (2003) 179–186.
[33] X. Zhang, Y.L. Chen, R.S. Liu, D.P. Tsai, Rep. Prog. Phys. 76 (2013) 046401.
[34] W.Y. Yang, S.W. Rhee, Appl. Phys. Lett. 91 (2007) 2907–2909.
[35] M.T. Greiner, M.G. Helander, Z.-B. Wang, W.-M. Tang, Z.-H. Lu, J. Phys. Chem. C 114 (2010) 19777–19781.
[36] M. Li, S. Zhou, Y. Zhang, G. Chen, Z. Hong, Appl. Surf. Sci. 254 (2008) 3762–3766.
[37] Y. Pan, S. Deng, L. Polavarapu, N. Gao, P. Yuan, C.H. Sow, Q.-H. Xu, Langmuir 28 (2012) 12304–12310.
[38] S.T. Kochuveedu, D.-P. Kim, D.H. Kim, J. Phys. Chem. C 116 (2011) 2500–2506.